



Integrated comparisons of thorium(IV) adsorption onto alkali-treated duckweed biomass and duckweed-derived hydrothermal and pyrolytic biochar

Ting Chen¹ · Nan Zhang¹ · Zhao Xu¹ · Xin Hu² · Zhuhong Ding¹

Received: 7 September 2018 / Accepted: 16 November 2018 / Published online: 24 November 2018
© Springer-Verlag GmbH Germany, part of Springer Nature 2018

Abstract

In order to remove aqueous radionuclides and find an appropriate method for the disposal of wild duckweed in eutrophic water body, alkali-treated duckweed biomass and duckweed-based hydrothermal biochar (hydrochar) and pyrolytic biochars of 300 and 600 °C were prepared. Their physicochemical properties were characterized carefully. The adsorption isothermal data fitted well with the Langmuir model and the maximum Langmuir adsorption capacities were 104.1, 96.3, 86.7, and 63.5 mg/g for hydrochar, modified biomass, and 300 and 600 °C biochars, respectively. The adsorption kinetic data fitted well with the pseudo-second-order kinetic equation. The sorption data of fixed-bed column also confirmed the high efficient removal of Th(IV) and fitted well with the Thomas model. The duckweed-based hydrothermal biochar is a low-cost adsorbent for Th(IV) removal, and it is also a resource utilization technology of the duckweed collected from eutrophic water body.

Keywords Radionuclide · Biosorbent · Biochar · Integrated characterization · Sorption

Introduction

Radionuclides present in the water have been considered to be a dangerous pollutant to destroy the normal function of cells and biological organisms by its self-decay (Huang et al. 2015). They may enter human tissue via respiratory system, digestive system, exposed skin, etc., and bring health risks to human (Abubakar Sadiq et al. 2015). The main sources of radioactive wastewater include nuclear power plants, research center of nuclear energy industry, medical institution, industrial produc-

tion, and university and research institution (Kaygun and Akyil 2007). The treatment of those wastewaters is generally compulsory before discharging into environmental media. Moreover, some natural water bodies also contain a small amount of thorium and it can migrate easily to groundwater (Humelnicu et al. 2004). Thorium (Th) is a naturally occurring radioactive element which is mainly distributed in the Earth's crust, and some human activities such as exploitation of ores with associated thorium and nuclear fuel reprocessing can also concentrate this element (Salinas-Pedroza and Olguín 2004). Thorium has also been extensively used in various applications such as the manufacture of high-strength alloys and UV photocells. These applications produce various gaseous, liquid and solid thorium, and uranium. Liquid wastes are discharged into the surface or ground waters of mines, causing water pollution and endangering the environment and human health. Therefore, studies on the removal of radionuclides including Th in water are particularly important.

The common techniques for the removal of radionuclides from water or wastewater include precipitation, micro-filtration, solvent extraction, adsorption, ion exchange, electrodialysis, and reverse osmosis (Rana et al. 2013). Among these techniques, adsorption is a highly effective and economical process. Some adsorbents and modified products of natural materials such as carboxylate-functionalized graft copolymer

Responsible editor: Tito Roberto Cadaval Jr

Electronic supplementary material The online version of this article (<https://doi.org/10.1007/s11356-018-3789-x>) contains supplementary material, which is available to authorized users.

✉ Zhuhong Ding
dzuhong@njtech.edu.cn

¹ School of Environmental Science and Engineering, Nanjing Tech University, 30 Puzhu Southern Road, Nanjing 211816, People's Republic of China

² State Key Laboratory of Analytical Chemistry for Life Science, Center of Material Analysis and School of Chemistry and Chemical Engineering, Nanjing University, 22 Hankou Road, Nanjing 210093, People's Republic of China

(Anirudhan et al. 2013), magnetite nanoparticles (Atta and Akl 2015), activated carbon (Kutahyali and Eral 2010), and calcined and flux calcined diatomite (Yusan et al. 2012) have been developed to remove radionuclides from water or wastewater. However, the development of novel, economical, and environment friendly adsorbents is still a challenge in adsorption. Biochar is a carbon-rich composite derived from biomass feedstock via slow pyrolysis in an oxygen-limited environment and has received increasing attention due to its multifunctionality including carbon sequestration, soil remediation/fertility enhancement, and novel adsorbents for wastewater treatment in recent years. Biochars derived from many biomass feedstock can efficiently remove aqueous Pb, Cu, Zn, Cd, and Cr (Ahmad et al. 2014; Inyang et al. 2016). Moreover, biosorbents have been widely used for biosorption of heavy metals and radionuclides (Wang and Chen 2014). For example, a *Pseudomonas* sp. has been investigated for the sequestration of uranium and thorium (Kazy et al. 2009). The integrated evaluation of the sorption of radionuclides onto modified biomass and its derivatives is also interesting in the development of novel, economical, and environment friendly adsorbents.

Duckweed is a common aquatic plant that is born in paddy fields, ponds, and other hydrostatic waters. It grows fast and is one of the common phytoplankton in eutrophic water body in China. Eutrophication is a serious environmental problem in most of rivers, lakes, and reservoirs in recent years in China. A lot of phytoplankton were salvaged as a method of eutrophication control; however, it is difficult to dispose them. Its resource utilization is an effective way to avoid the secondary pollution. The development of the wild duckweed as low-cost sorbents may be a novel, economical, and environment friendly resource utilization. Biomass of wild duckweed was used as a biosorbent after alkali pretreatment to remove soluble compounds. Biochars were also prepared from the wild duckweed via hydrothermal method and slow pyrolysis at 300 and 600 °C, respectively. The resultant sorbents were characterized. Static batch and dynamic column adsorption experiments were carried out. The objective of this study is to evaluate the sorption performance and mechanisms of thorium(IV) onto the resultant biosorbent, hydrothermal, and pyrolytic biochars prepared from wild duckweed to develop novel, economical, and environment friendly adsorbents for the removal of radionuclides. It is a helpful attempt to develop a novel and sustainable strategy for resource disposal of phytoplankton for eutrophication control.

Materials and methods

Materials and reagents

Wild duckweed was collected from Xuanwu Lake in Nanjing, China. Duckweed was washed after collection to remove

impurities. Chemical reagents of analytic grade including NaOH, HCl, HNO₃, and Th(NO₃)₄ were purchased from Nanjing Chemical Reagent Co. All solutions used in the experiment were prepared with deionized (DI) water (18.2 MΩ/cm).

Preparation of biochars and modified biomass

- 1) Hydrothermal biochar (*hydrochar*). The washed fresh duckweed was placed in a 250-ml stainless steel hydrothermal reaction kettle and mixed with 100 ml of deionized water. The reaction kettle was sealed with cap and placed in a constant temperature heating box at 200 °C for 12 h. The product was taken out for filter washing and then dried in a constant temperature oven at 80 °C. The resulting biochar was sieved through 60-mesh nylon sieve after smashing, and then placed in a polyethylene plastic ziplock bag. The resulting biochar was recorded as BC-W.
- 2) Pyrolytic biochars. The washed fresh duckweed was placed in an electric blast drying oven at 80 °C until dried; then, the feedstock was pyrolyzed in a tube furnace under pyrogenic conditions at 300 and 600 °C, respectively. The resulting biochars were sieved with 60-mesh nylon sieve, and then marked as BC-300 and BC-600, respectively.
- 3) Modified biomass. Dried biomass was immersed in 0.1 M NaOH solution for 24 h (1:50 w:v). The modified biomass was filtered and washed with deionized water for several times until nearly neutral pH, and then dried in an electric blast drying oven at 80 °C, and finally sieved with 60-mesh nylon sieve, noted as BM-M.

Characterization of biochar and modified biomass

A CHN Elemental Analyzer (Carlo-Erba, NA-1500) was used to measure the contents of C, H, and N in biochar and modified biomass, and the content of O was calculated according to the result. The determination of ash content referred to the method of “GB/T 12496.3–1999.” The pH of the point of zero charge, pH_{PZC}, was determined using the modified drift method (Kosmulski 2009). Mineral elements were determined using an inductively coupled plasma–optical emission spectroscopy (ICP-OES; PerkinElmer Optima 5300 DV, USA). Specific surface area was measured with nitrogen adsorption methods through a surface area analyzer (BET; Tristar 3300, Micromeritics, USA). The curves of thermogravimetry (TG/DTG) were fitted by a NETZSCH TGA/DSC thermogravimetric analyzer (TGA/DSC; STA449F3, NETZSCH, GER) under N₂ and O₂ atmosphere, respectively. The functional groups were analyzed by a Fourier transform infrared spectrometer (FT-IR; NEXUS870, Nicolet, USA). A scanning electron microscopy (SEM; S-3400N II, Hitachi, JP) was used

to observe its surface morphology and particle size. Analysis of crystal phase structure was carried out by an X-ray diffractometer (XRD; X'TRA, ARL, Switzerland).

Adsorption experiments

Isotherm adsorption The pH-dependent distribution of Th(IV) of 75 mg/L at 25 °C was simulated by using Visual MINTEQ version 3.1. Th(IV) is the main species below pH 3.0 and with the increasing solution pH, species of Th(IV) change to $\text{Th}(\text{OH})^{+3}$ and $\text{Th}(\text{OH})_2^{+2}$; therefore, experimental solution pH in the present study was set as 2.7. The isothermal adsorption experiments were designed to determine the effect of initial concentration on equilibrium adsorption. According to the pre-experiment, the initial concentrations of Th(IV) were set as 1, 5, 10, 25, 50, 75, and 100 mg/L, and the pH of solution was adjusted to about 2.7. Of the duckweed-based biochar and modified biomass samples, 0.0100 g was placed in 50-ml polyethylene centrifuge tubes, and then mixed with 20 ml Th(IV) solution. The mixture was rotated 24 h at 10 rpm at room temperature (22 ± 2 °C) to ensure complete equilibrium adsorption. The samples were centrifuged at 4200 rpm for 5 min, and then, the supernatant was filtered through 0.22- μm membrane filter. Five-milliliter solution was stored for the analyses of Th(IV) by using an ICP-OES (Optima 5300, PerkinElmer, USA). The mass of sorbed Th(IV) per unit sorbent mass were calculated based on the differences between initial and final aqueous solution concentrations.

Adsorption kinetics According to pre-test and adsorption isotherm experiments, the initial concentration of Th(IV) was set as 75 mg/L and the pH was adjusted to 2.7. Of the duckweed-based biochar or modified biomass, 0.0100 g was put in 50-ml round bottom screw plastic centrifuge tube, and then 20 ml of Th(IV) solution with the initial concentration of 75 mg/L was added. The contact time was set as 1, 10, 30, 60, 120, 240, 480, 720, and 1440 min on the turntable, respectively. The samples after the arrival of the designed time were removed for centrifugation at 4200 rpm for 5 min. The supernatant was filtered through a 0.22- μm filter. The concentrations of Th(IV) after adsorption in the filtered solution were determined by using the ICP-OES. The mass of sorbed Th(IV) per unit sorbent mass was calculated based on the differences between initial and final aqueous solution concentrations.

Column adsorption Column adsorption for Th(IV) removal was carried out. Briefly, 0.300 g of BC-W, BC-300, BC-600, and BM-M were, respectively, packed in the middle of an acrylic column with an inner diameter of 1.5 cm. The upper and lower ends of the adsorption column were filled with acid-washed quartz sand (average particle size 0.5–0.6 mm) to help distribution of the flow. The 300-mesh sieve was filled between biochar and quartz sand to prevent biochar from being carried out by the flow. A peristaltic pump (Masterflex L/S,

Cole Parmer Instrument, Vernon Hills, IL) was used at the influent (bottom) of the column to maintain an upward flow rate in the column of 1 mL/min. Before test, the deionized water was injected through the adsorption column to remove possible impurities in biochars and biomass. Column effluent was collected by a fraction collector (IS-95 Interval Sampler, Spectrum Chromatography, Houston, TX). The flow rate of the peristaltic pump was adjusted to the corresponding flow rate and the collection time was set to make sure 2 ml solution collected every time. The concentrations of Th(IV) in the leachate were analyzed by using the ICP-OES. Persistent influent of 500 mg/L Th(IV) solution (pH 2.7) was injected for 100 min. The mass of sorbed Th(IV) per unit sorbent mass was calculated based on the differences between initial and final aqueous solution concentrations.

Results and discussion

Physiochemical properties of biochar and modified biomass

Yield and contents of ash, C, H, O, and N of the four adsorbents are shown in Table 1. The yield of pyrolytic biochar decreased with the increase of pyrolysis temperature (Table 1). It is consistent with the previous reports (Lee et al. 2015; Uchimiya et al. 2011). As the temperature rises, cellulose and hemicellulose degraded, the organic components in the biochars underwent deoxygenation and dehydrogenation, and the volatile components were released. The yield of hydrothermal biochar was lower than that of pyrolysis biochar (Table 1). Ash contents of adsorbents except for BC-600 were lower than 30%. The modified biomass (BM-M) had the lowest ash content of 16.9% and the BC-600 had the highest ash content of 43.5% (Table 1). This was because when the pyrolysis temperature increased, the organic components in the biochar degraded, resulting in an increase in ash content. As for the pyrolytic biochars, the ash content was related to the carbonization temperature. The comparisons showed that the specific surface area of BC600 with high pyrolysis temperature (600 °C) were larger than that of BC-300 with low pyrolysis temperature (300 °C), which was consistent with the literature reports (Ronsse et al. 2013; Xu et al. 2017). BM-M had the lowest specific surface area. Compared with the *pyrolytic* biochars, *hydrothermal* biochar (BC-W) had lower surface area, which is also consistent with the reported studies (Garlapalli et al. 2016; Mumme et al. 2011). It could be found from Table 1 that the carbon content in the biochar was much higher than that in the modified biomass, and increased with the increasing pyrolysis temperature. The content of H and O reduced compared to the modified biomass, suggesting that the dehydroxylation effect during the formation of biochar was also obvious (Demirbas 2004). H/C can reflect the

Table 1 Specific surface area, yields (%), ash contents (AC), and elemental compositions of biochars and modified biomass

| | BET m ² /g | Yields % | AC | C | H | O | N | H/C | K mg/g | Ca | Mg | Na |
|--------|--------------------------|-------------|------|------|------|------|-------|-------|-----------|-----|------|------|
| BC-W | 8.10 | 35.5 | 19.8 | 47.8 | 5.29 | 26.7 | 0.440 | 0.111 | 19.2 | 158 | 12.9 | 4.73 |
| BC-300 | 3.63 | 53.7 | 24.5 | 47.6 | 4.01 | 19.2 | 4.74 | 0.084 | 63.3 | 134 | 32.6 | 10.0 |
| BC-600 | 6.72 | 37.8 | 43.5 | 49.2 | 1.45 | 3.53 | 2.32 | 0.029 | 94.2 | 130 | 27.2 | 17.5 |
| BM-M | 1.65 | / | 16.9 | 38.3 | 5.63 | 37.1 | 2.07 | 0.147 | 4.89 | 186 | 21.7 | 23.9 |

content of aromatic C (Xiao et al. 2016). In the current study, with the increase of pyrolysis temperature, the H/C atomic ratio decreased, indicating that the higher the pyrolysis temperature is, the more obvious the aromatization of biochar was. Mineral elements are also an important part of biochar. The result in Table 1 illustrated that mineral composition of biochars prepared with different pyrolytic temperature were different.

pH_{PZC} is an important index for adsorption performance of adsorbent. When the pH of the solution is lower than the value of pH_{PZC} of the adsorbent, the surface of the adsorbent is positively charged, and it favors the adsorption of the anionic contaminant; when the pH of the solution is higher than pH_{PZC} of the adsorbent, the surface is negatively charged and it favors the adsorption of the cationic contaminant (Jiménez-Cedillo et al. 2013). In this paper, the pH_{PZC} of duckweed-based biochars and modified biomass is shown in Fig. S1. The pH_{PZC} of BC-W, BC-300, BC-600, and BM-M were 5.98, 7.26, 10.18, and 8.79, respectively (Fig. S1). Therefore, biochars with higher pyrolysis temperatures (BC-600) had higher pH_{PZC} values, and BC-W had the lowest point of zero charge.

The thermal stability of the resulting sorbents can be analyzed with a thermogravimetric analyzer. TGA/DTG curves under N₂ and O₂ atmosphere are presented in Fig. 1. According to the peaks of DTG curves of Fig. 1a, mass loss process of biochars and biomass could be divided into three stages. The first stage was in the temperature range from 100 to 200 °C, and the mass loss may be caused by evaporation of water and a small amount of volatile substances. The second stage was in the temperature range from 200 to 400 °C, and

gradual degradation of the cellulose, hemicellulose, and other organic functional groups in samples led to the loss (Hernandez-Mena et al. 2014). The maximum mass loss rate of BM-M reached 4.5%/°C and the corresponding temperature was about 310 °C, while that of BC-W was 0.36%/°C and the corresponding temperature was about 330 °C, which indicated the different flammability of biochars and biomass (Hu et al. 2015). The third stage was in the range from 400 to 550 °C, in which the mass loss was mainly caused by the degradation of stable lignin (Yang et al. 2004). The curves of TGA showed that the percentage of mass to initial mass followed the order of BM-M > BC-W > BC-300 > BC-600. The maximum loss was observed on the modified biomass (about 70%) while BC-600 had only 10% loss. These indicated that the biochar with high pyrolysis temperature had strong thermal stability. It could be seen from Fig. 1b that ignition points of four samples differed greatly. Pyrolytic biochars (BC-300 and BC-600) had relatively high ignition points while ignition point of BM-M was the lowest. Therefore, they had different oxidation resistance.

The surface functional groups of the adsorbents were analyzed by using a Fourier transform infrared spectroscopy (Fig. 2). The peak appearing at 3400 cm⁻¹ was generated by stretching vibration of hydroxyl O–H groups (alcohols, phenols) (Guo et al. 2008). The peak of 1600 cm was related to the stretching vibration of carboxyl –COOH. However, neither of the peak occurred in infrared spectrum of BC-600, indicating that the high pyrolysis temperature resulted in the decrease of the carboxyl and hydroxyl groups of biochar. In the vicinity of 1062 cm⁻¹, the telescopic vibration peak of the aromatic C–O was observed (Ding et al. 2016), and the peak

Fig. 1 Thermogravimetric and differential thermogravimetric (TGA/DTG) curves of the studied adsorbents under N₂ (a) and O₂ (b) atmosphere

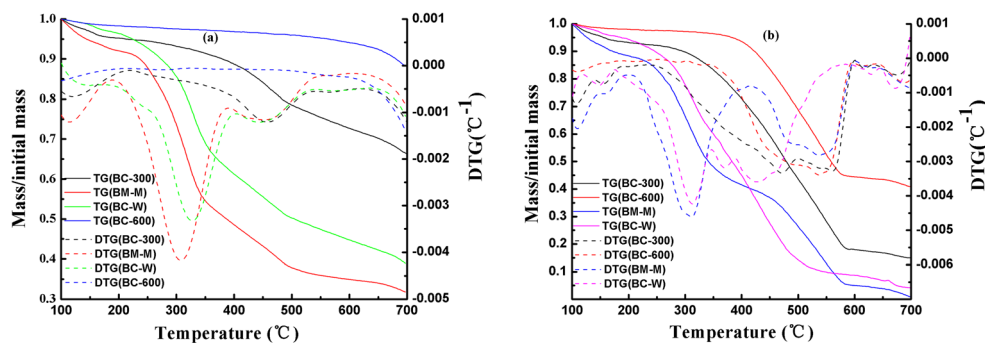
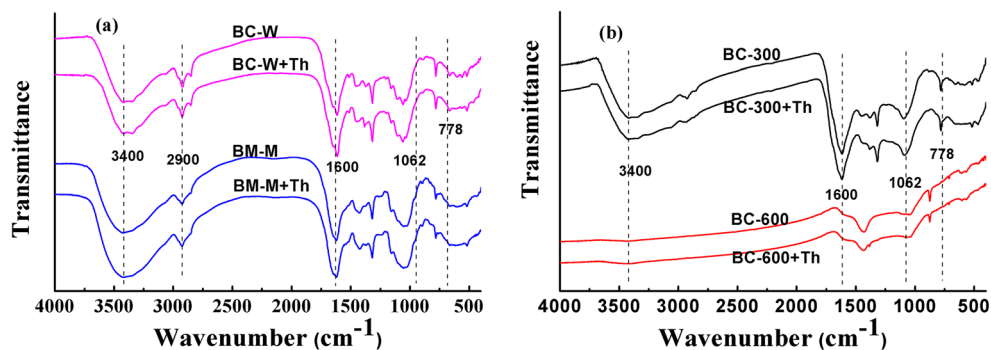


Fig. 2 FT-IR spectra of biochars and modified biomass before and after adsorption of Th(IV)



of BC-600 was significantly lower than that of the other adsorbents. The peak appearing near 778 cm^{-1} was the bending vibration peak of CO_3^{2-} , indicating mineral carbonates in duckweed-based biochars and modified biomass (Xu et al. 2013). Moreover, there were no significant differences among the infrared spectra of BM-M, BC-W, and BC-300, which suggested their similar functional groups. In a word, BM-M, BC-W, and BC-300 could provide abundant oxygen-containing functional groups, which was benefit for the sorption of aqueous thorium (Th) ions. The FT-IR spectra of Th(IV)-sorbed adsorbents were similar to those of pristine adsorbents, suggesting that no new peaks or obvious shift effects were observed. It may be due to the intense light absorption of black biochar masking the tiny FT-IR displacement effect or caused by the limited Th(IV) adsorption (Ding et al. 2017; Yang et al. 2014).

X-ray diffraction is a suitable technique for analyzing the crystalline structure of biochar and the crystallinity of biomass (Ertaş and Alma 2010). The XRD spectra of the adsorbents are shown in Fig. S2. There were two distinct peaks in BM-M, BC-W and BC-300 spectra at 2θ of 15° and 23° , which were related to the crystal structure of cellulose in duckweed-based biochar according to the research of Keiluweit et al. (2010). They disappeared in BC-600 spectrum, indicating that the cellulose components were degraded at high temperature (Jiang et al. 2007; Kim et al. 2012). A narrow peak at the 2θ values of around 26.6° was assigned to SiO_2 (Jindo et al. 2014). In addition, a considerable amount of potassium signal peaks appeared at 28.3° and 40.5° . The biochar contained a small amount of calcium carbonate according to the low peak appeared at 29.4° (Yuan et al. 2011). XRD spectrum of the Th(IV)-sorbed biochars and modified biomass (Fig. S2) showed that there was no obvious changes compared with the pristine adsorbents, which indicated that no new precipitate was detected after adsorption of Th(IV), and the precipitation might not be the main mechanism for the adsorption of Th(IV) onto the adsorbents.

Raman spectroscopy is an effective characterization technique to study the crystalline and amorphous carbon in biochar materials (Robertson 2004). Defect band (D) are ascribed to a

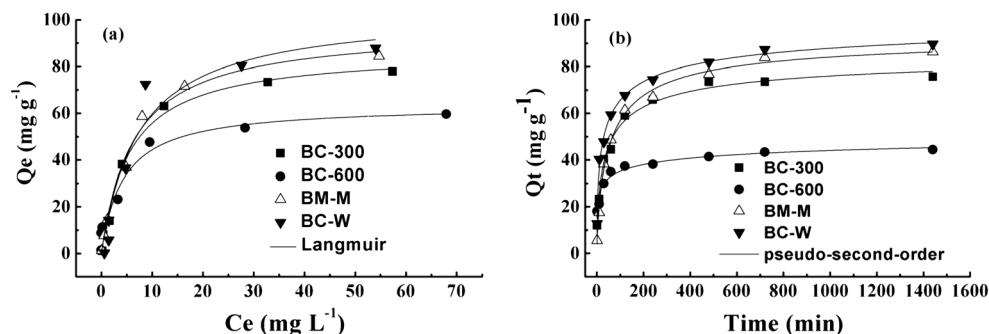
mixture of symmetric breathing modes of disordered graphite rings and Kekule-type vibrations in larger ring systems (Chia et al. 2012; Smith et al. 2016). Band (G) represents vibrations of sp^2 -bonded configurations and C=C double bonds found in graphitic carbon, with smaller band gap (Smith et al. 2016). The ratio of D band intensity to G band intensity (ID/IG) reflects the graphitization degree (Chen et al. 2015). Also, ID/IG is considered to be inversely proportional to the degree of ordering of the carbon structure. The Raman spectra of the adsorbents are shown in Fig. S3. There were no peaks in spectra of BC-W, BC-300 and BM-M in the D and G regions, suggesting no graphitization. Two sharp Raman spectral peaks (D and G bands) were observed in the spectra of BC-600, suggesting that aromatic carbon and graphite had formed in the biochar. ID/IG was 1.921 for BC-600 in Fig. S4, indicating the ordering of the carbon structure for BC-600.

The scanning electron microscope images of the adsorbents are presented in Fig. S4. It can be observed from Fig. S4 that the pores of biochars were dense, open, and honeycomb shaped. Compared with Fig. S4a, Fig. S4b, c shows that the increasing pyrolysis temperature improved the coarseness, delamination degree, and pore structure of biochars. This was due to the fact that during pyrolysis, a lot of holes appeared in the structure with the decomposition and consumption of organic matter, making the biochar overall porous. Figure S4d illustrates that there was a much more rough and complex pore structure with a content of minerals and inorganic compounds in the surface of biomass.

Adsorption isotherm

The effects of initial concentration of Th(IV) on the adsorption onto the studied adsorbents are shown in Fig. 3a. The adsorption capacities of the adsorbents were similar at low initial concentrations of Th(IV), increased with the increasing initial Th(IV) concentrations, and then arrived at a near platform (Fig. 3a). BC-W had the highest adsorption capacity while BC-600 had the lowest (Fig. 3a). To better understand the adsorption process, Langmuir, Freundlich, and Dubinin–Radushkevich isotherm models were used to fit the

Fig. 3 Adsorption isotherms (a) and kinetics (b) of Th(IV) onto the studied adsorbents



experimental data (Table S1, supporting information). The correlation coefficient (R^2) indicates that Langmuir model fitted the experimental data better than Freundlich model, suggesting the monolayer adsorption. As for Langmuir model, a dimensionless constant of the separation factor (R_L , $R_L = 1/(1 + K_L \times C_0)$) classifies the adsorption to be unfavorable ($R_L > 1$), favorable ($0 < R_L < 1$), and linear ($R_L = 1$) or irreversible ($R_L = 0$) (Abd El-Latif and Elkady 2010). The values of R_L were all in the range of 0 and 1, suggesting the favorable adsorption of Th(IV). It is consistent with the constant of $1/n$ of Freundlich model that the favorable adsorption of Th(IV) was indicated due to $1/n < 1$ (Table S1). Dubinin–Radushkevich (D-R) model is usually used to distinguish adsorption process of chemical or physical. The parameter β of D-R model is closely related to the mean free energy E ($E = 1/\sqrt{2\beta}$), which was generated when Th ions were transferred from solution to adsorbents in the experiment. If $E < 8$ kJ/mol, the adsorption process is physical, and the value in the range from 8 to 16 kJ/mol indicated the chemical adsorption (Shin and Kim 2016). The value of E in Table S1 was between 1.08 and 5.66, which gave the information that the adsorption process of Th(IV) was physical adsorption. Moreover, Table S2 lists the maximum adsorption capacity for Th(IV) in the previous literatures. Compared with these results, the maximum adsorption capacities of our studied adsorbents for thorium were similar or above them, suggesting that the duckweed-based adsorbent was low-cost and effective for the removal of Th(IV).

Adsorption kinetics

The adsorption kinetics of the studied adsorbents for Th(IV) are shown in Fig. 3b. Figure 3b shows that the adsorption process for Th(IV) included two stages: rapid adsorption in the early stage and slow adsorption in the late stage, which was determined by adsorption sites on the surface of biochars and modified biomass. In the early stage, Th(IV) ions occupied the adsorption sites quickly, the adsorption sites on the surface of the adsorbent decreased, and then, the adsorption

rate slowed down and finally tended to be stable at about 840 min.

Pseudo-first-order and pseudo-second-order kinetic equations were used to fit the experimental data, and parameters are listed in Table S3. The coefficients (R^2) showed that the pseudo-second-order kinetic model fitted the experimental data better than the pseudo-first-order kinetic equation (Table S3). In order to understand the rate-limiting steps in the adsorption process, Weber and Morris intraparticle diffusion model was introduced (Table S3). The Weber and Morris intraparticle diffusion of adsorbents is shown in Fig. 4. The plot of q_t was not very linear to $t^{1/2}$, which could also be confirmed from R^2 (0.700–0.768) in Table S3. The plots did not pass through the origin which indicated that liquid film diffusion was not the only rate-limiting step in the adsorption process. The whole plots could be divided into three linear portions. The first linear portion was controlled by liquid film diffusion, with the fastest adsorption rate; Th(IV) ion was transferred to the external surface of studied adsorbents. In the second linear portion, the Th(IV) entered into the pores of the adsorbents by intraparticle diffusion which was a rate-limiting step. The third portion was a dynamic balancing

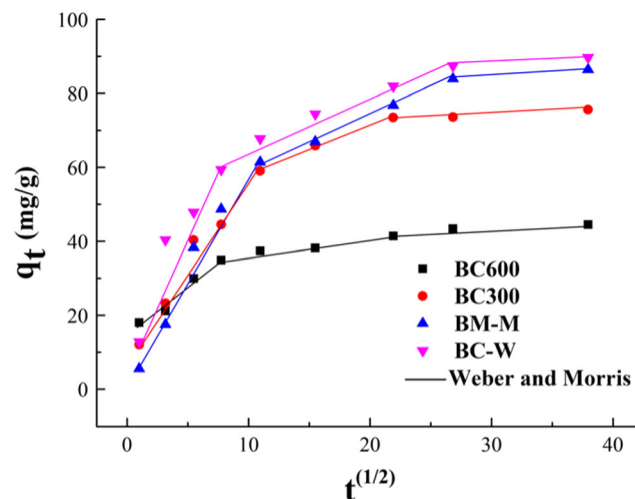


Fig. 4 The Weber and Morris intraparticle diffusion for the adsorption of Th(IV) by four kind of adsorbents

process, when Th(IV) occupied all the active sites of the adsorbent and the maximum adsorption was reached, and the adsorption rate slowdown and became stagnant.

Column adsorption

The breakthrough curves of Th(IV) in adsorption column are shown in Fig. 5. The initial concentration of Th(IV) was set as 500 mg/l and the flow rate was 1 ml/min. The breakthrough curve could generally be divided into three phases. In the first phase (the beginning of curve “S”, Th(IV) injected into column was adsorbed by the studied sorbents. The adsorption sites were far from saturation, so the effluent concentration was approximately 0 ($C_t/C_0 \approx 0$). In the second phase (the middle of curve S), sites of the adsorbents in column reached the adsorption saturation step by step, so the effluent concentration of Th(IV) began to increase (increasing C_t/C_0). Breakthrough occurred at this phase. When the sorbate emerges from the outflow, the corresponding point of the breakthrough curve is called the breakthrough point. In the current experiment, the effluent volume at the breakthrough points was 12, 20, 16, and 10 ml for BC-W, BC-600, BC-300, and BM-M, respectively, but the adsorption was still not fully saturated. In the third phase (the ending of S), the studied sorbents in the adsorption column reached the adsorption saturation (i.e., $C_t/C_0 = 1$) when the effluent volume was 70, 94, 50, and 64 ml for BC-W, BC-600, BC-300, and BM-M, respectively.

In order to understand the column adsorption, the adsorption data were fitted with the Thomas model. The specific parameters were shown in Table S4. The experimental adsorption capacity of BC-600 was 73.8 mg/g and the theoretical adsorption capacity was 71.7 mg/g. The actual adsorption capacities of BC-W, BC-300, and BM-M were 55.8, 38.7, and 47.1 mg/g, respectively, and the corresponding theoretical adsorption capacities were 47.4, 33.7, and 38.3 mg/g. So the adsorption

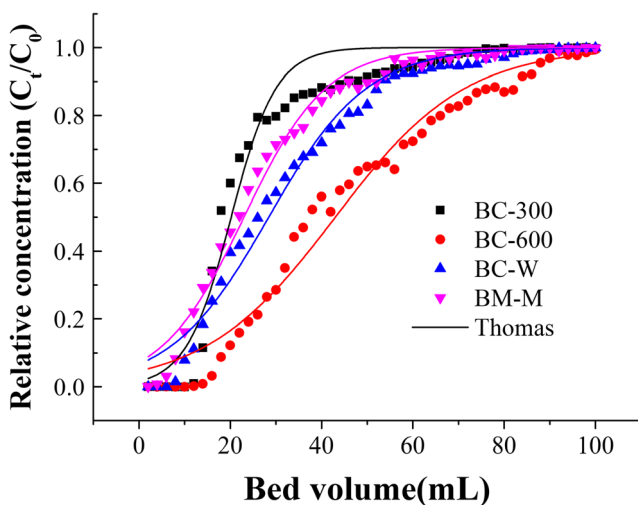


Fig. 5 The breakthrough curves of Th(IV) in fixed-bed column packed with biochars and modified biomass

capacities were in the order of BC-600 > BC-W > BM-M > BC-300, which was not consistent with the batch adsorption data. From the kinetic adsorption of batch experiments (Fig. 3b), the whole adsorption rate for the whole process was relatively slow (about 200–400 min) and BC-600 had the fastest rate. For column experiment, the flowing supply of Th(IV) may resulted in insufficient contact time to arrive at the maximum adsorption capacities of batch experiments for Th(IV) when $C_t/C_0 = 1$ (100 min for the whole column experiments). So BC-600 was easy to arrive at the maximum adsorption capacities due to its faster adsorption rate.

Duckweed is a typical phytoplankton in eutrophic water body and fresh duckweed contains abundant water (over 90%). To the preparation of hydrothermal biochar and biosorbent (modified biomass), the step of drying can be omitted, which will save the cost compared with pyrolytic biochars. Taking the adsorption capacities of batch and column adsorption and run cost into account, the duckweed-based hydrothermal biochar was the appropriate adsorbent in this study.

Conclusions

The physicochemical properties of hydrothermal biochar, modified biomass, and pyrolytic biochar of 300 and 600 °C differed greatly. The maximum Langmuir adsorption capacities were 104.1, 96.3, 86.7, and 63.5 mg/g for hydrothermal biochar, modified biomass, and pyrolytic biochar of 300 and 600 °C, respectively. Adsorption isothermal and kinetic data fitted well with the Langmuir equation and the pseudo-second-order kinetic equation, respectively. Column sorption confirmed the efficient removal of Th(IV). The duckweed-based hydrothermal biochar is suggested as an appropriate adsorbent for Th(IV) removal, and the resource disposal of duckweed in the eutrophic water as an adsorbent is a novel and sustainable strategy.

Funding The work was supported by the National Natural Science Foundation of China (No. 21677075) and the Project of International Cooperation and Exchange of Nanjing Tech University (2017–2019).

References

- Abd El-Latif MM, Elkady MF (2010) Equilibrium isotherms for harmful ions sorption using nano zirconium vanadate ion exchanger. *Desalination* 255:21–43
- Abubakar Sadiq A, Umar I, Chidozie Timothy A, Nuraddeen Nasiru G, Ahmad Termizi R (2015) Health and ecological hazards due to natural radioactivity in soil from mining areas of Nasarawa state, Nigeria. *Isot Environ Health Stud* 51:448–468
- Ahmad M, Rajapaksha AU, Lim JE, Zhang M, Bolan N, Mohan D, Vithanage M, Lee SS, Ok YS (2014) Biochar as a sorbent for contaminant management in soil and water: a review. *Chemosphere* 99: 19–33

- Anirudhan TS, Sreekumari SS, Jalajamony S (2013) An investigation into the adsorption of thorium(IV) from aqueous solutions by a carboxylate-functionalised graft copolymer derived from titanium dioxide-densified cellulose. *J Environ Radioact* 116:141–147
- Atta AM, Akl ZF (2015) Removal of thorium from water using modified magnetite nanoparticles capped with rosin amidoxime. *Mater Chem Phys* 163:253–261
- Chen C, Zhou W, Lin D (2015) Sorption characteristics of N-nitrosodimethylamine onto biochar from aqueous solution. *Bioresour Technol* 179:359–366
- Chia CH, Gong B, Joseph SD, Marjo CE, Munroe P, Rich AM (2012) Imaging of mineral-enriched biochar by FTIR, Raman and SEM-EDX. *Vib Spectrosc* 62:248–257
- Demirbas A (2004) Effects of temperature and particle size on bio-char yield from pyrolysis of agricultural residues. *J Anal Appl Pyrolysis* 72:243–248
- Ding Z, Wan Y, Hu X, Wang S, Zimmerman AR, Gao B (2016) Sorption of lead and methylene blue onto hickory biochars from different pyrolysis temperatures: importance of physicochemical properties. *J Ind Eng Chem* 37:261–267
- Ding ZH, Wu HL, Hu X (2017) Multiple characterization for mechanistic insights of Pb(II) sorption onto biochars derived from herbaceous plant, biosolid, and livestock waste. *Bioresources* 12:6763–6772
- Ertas M, Alma MH (2010) Pyrolysis of laurel (*Laurus nobilis* L.) extraction residues in a fixed-bed reactor: characterization of bio-oil and bio-char. *J Anal Appl Pyrolysis* 88:22–29
- Garlapalli RK, Wirth B, Reza MT (2016) Pyrolysis of hydrochar from digestate: effect of hydrothermal carbonization and pyrolysis temperatures on pyrochar formation. *Bioresour Technol* 220:168–174
- Guo X, Zhang S, Shan XQ (2008) Adsorption of metal ions on lignin. *J Hazard Mater* 151:134–142
- Hernandez-Mena LE, Pecora AAB, Beraldo AL (2014) Slow pyrolysis of bamboo biomass: analysis of biochar properties. *Chem Eng Trans* 37:115–120
- Hu X, Ding ZH, Zimmerman AR, Wang SS, Gao B (2015) Batch and column sorption of arsenic onto iron-impregnated biochar synthesized through hydrolysis. *Water Res* 68:206–216
- Huang YJ, Chen CF, Huang YC, Yue QJ, Zhong CM, Tan CJ (2015) Natural radioactivity and radiological hazards assessment of bone-coal from a vanadium mine in Central China. *Radiat Phys Chem* 107:82–88
- Humelnicu D, Drochioiu G, Popa K (2004) Bioaccumulation of thorium and uranyl ions on *Saccharomyces cerevisiae*. *J Radioanal Nucl Chem* 260:291–293
- Inyang MI, Gao B, Yao Y, Xue YW, Zimmerman A, Mosa A, Pullammanappallil P, Ok YS, Cao XD (2016) A review of biochar as a low-cost adsorbent for aqueous heavy metal removal. *Crit Rev Environ Sci Technol* 46:406–433
- Jiang ZH, Yang Z, So CL, Hse CY (2007) Rapid prediction of wood crystallinity in *Pinus elliotii* plantation wood by near-infrared spectroscopy. *J Wood Sci* 53:449–453
- Jiménez-Cedillo MJ, Olguín MT, Fall C, Colin-Cruz A (2013) As(III) and as(V) sorption on iron-modified non-pyrolyzed and pyrolyzed biomass from *Petroselinum crispum* (parsley). *J Environ Manag* 117:242–252
- Jindo K, Mizumoto H, Sawada Y, Sanchezmonedero MA, Sonoki T (2014) Physical and chemical characterization of biochars derived from different agricultural residues. *Biogeosci Discuss* 11:6613–6621
- Kaygun AK, Akyil S (2007) Study of the behaviour of thorium adsorption on PAN/zeolite composite adsorbent. *J Hazard Mater* 147:357–362
- Kazy SK, D'Souza SF, Sar P (2009) Uranium and thorium sequestration by a *Pseudomonas* sp.: mechanism and chemical characterization. *J Hazard Mater* 163:65–72
- Keiluweit M, Nico PS, Johnson MG, Kleber M (2010) Dynamic molecular structure of plant biomass-derived black carbon (biochar). *Environ Sci Technol* 44:1247–1253
- Kim KH, Kim JY, Cho TS, Choi JW (2012) Influence of pyrolysis temperature on physicochemical properties of biochar obtained from the fast pyrolysis of pitch pine (*Pinus rigida*). *Bioresour Technol* 118:158–162
- Kosmulski M (2009) pH-dependent surface charging and points of zero charge. IV. Update and new approach. *J Colloid Interface Sci* 337:439–448
- Kutahyalı C, Eral M (2010) Sorption studies of uranium and thorium on activated carbon prepared from olive stones: kinetic and thermodynamic aspects. *J Nucl Mater* 396:251–256
- Lee SJ, Jin HP, Ahn YT, Chung JW (2015) Comparison of heavy metal adsorption by Peat Moss and Peat Moss-derived biochar produced under different carbonization conditions. *Water Air Soil Pollut* 226(2):1–11
- Mumme J, Eckervogt L, Pielert J, Diakité M, Rupp F, Kern J (2011) Hydrothermal carbonization of anaerobically digested maize silage. *Bioresour Technol* 102:9255–9260
- Rana D, Matsuura T, Kassim MA, Ismail AF (2013) Radioactive decontamination of water by membrane processes — a review. *Desalination* 321:77–92
- Robertson J (2004) Raman spectroscopy of amorphous, nanostructured, diamond-like carbon, and Nanodiamond. *Philos Trans Math Phys Eng Sci* 362:2477–2512
- Ronsse F, Sv H, Dickinson D, Prins W (2013) Production and characterization of slow pyrolysis biochar: influence of feedstock type and pyrolysis conditions. *Glob Change Biol Bioenergy* 5:104–115
- Salinas-Pedroza MG, Olguín MT (2004) Thorium removal from aqueous solutions of Mexican erionite and X zeolite. *J Radioanal Nucl Chem* 260:115–118
- Shin HS, Kim JH (2016) Isotherm, kinetic and thermodynamic characteristics of adsorption of paclitaxel onto Diaion HP-20. *Process Biochem* 51:917–924
- Smith MW, Dallmeyer I, Johnson TJ, Brauer CS, McEwen JS, Espinal JF, Garcia-Perez M (2016) Structural analysis of char by Raman spectroscopy: improving band assignments through computational calculations from first principles. *Carbon* 100:678–692
- Uchimiya M, Wartelle LH, Klasson KT, Fortier CA, Lima IM (2011) Influence of pyrolysis temperature on biochar property and function as a heavy metal sorbent in soil. *J Agric Food Chem* 59:2501–2510
- Wang JL, Chen C (2014) Chitosan-based biosorbents: modification and application for biosorption of heavy metals and radionuclides. *Bioresour Technol* 160:129–141
- Xiao X, Chen ZM, Chen BL (2016) H/C atomic ratio as a smart linkage between pyrolytic temperatures, aromatic clusters and sorption properties of biochars derived from diverse precursory materials. *Sci Rep-Uk* 6:1–13
- Xu X, Cao X, Zhao L (2013) Comparison of rice husk- and dairy manure-derived biochars for simultaneously removing heavy metals from aqueous solutions: role of mineral components in biochars. *Chemosphere* 92:955–961
- Xu X, Hu X, Ding Z, Chen Y (2017) Effects of copyrolysis of sludge with calcium carbonate and calcium hydrogen phosphate on chemical stability of carbon and release of toxic elements in the resultant biochars. *Chemosphere* 189:76–85
- Yang HP, Yan R, Chin T, Liang DT, Chen HP, Zheng CG (2004) Thermogravimetric analysis-Fourier transform infrared analysis of palm oil waste pyrolysis. *Energy Fuel* 18:1814–1821
- Yang Y, Wei ZB, Zhang XL, Chen X, Yue DM, Yin Q, Xiao L, Yang LY (2014) Biochar from *Alternanthera philoxeroides* could remove Pb(II) efficiently. *Bioresour Technol* 171:227–232
- Yuan JH, Xu RK, Zhang H (2011) The forms of alkalis in the biochar produced from crop residues at different temperatures. *Bioresour Technol* 102:3488–3497
- Yusan S, Gok C, Erenturk S, Aytas S (2012) Adsorptive removal of thorium (IV) using calcined and flux calcined diatomite from Turkey: evaluation of equilibrium, kinetic and thermodynamic data. *Appl Clay Sci* 67-68:106–116